Measurement 151 (2020) 107171

Contents lists available at ScienceDirect

Measurement

journal homepage: www.elsevier.com/locate/measurement

Spatial frequency domain analysis of a commercially available digital dental detector

A. Anastasiou [a], F. Papastamati [a], A. Bakas [b], C. Michail [a], V. Koukou [a], N. Martini [a], K. Ninos [b], E. Lavdas [b], I. Valais [a], G. Fountos [a], I. Kandarakis [a], N. Kalyvas [a,*]

[a] Department of Biomedical Engineering, University of West Attica, 12243, Egaleo, Athens, Greece
[b] Department of Biomedical Sciences, University of West Attica, 12243, Egaleo, Athens, Greece

ARTICLE INFO

Article history:
Received 18 March 2019
Received in revised form 8 October 2019
Accepted 15 October 2019
Available online 18 October 2019

Keywords:
Dental detector
CMOS
SCHICK CDR
DQE

ABSTRACT

X-ray detectors are used in medical imaging for the representation of diagnostic information. Digital detector performance is evaluated through appropriate parameters in the spatial domain (i.e. contrast, noise or resolution) and in the frequency domain. Dental radiography is a domain of medical imaging. The purpose of this work is the examination of a commercially available digital dental imaging detector through spatial frequency domain parameters. The available detector was a commercially available image receptor SCHICK CDR, working in indirect mode that is a scintillator coupled to a Complementary Metal Oxide Semiconductor (CMOS) photoreceptor. The detector was irradiated at an X-ray system with 60 kVp and 70 kVp tube voltages utilized in intraoral radiography. The detector linearity, Modulation Transfer Function (MTF), Normalized Noise Power Spectrum (NNPS) and Detective Quantum Efficiency (DQE) were measured according to literature. The Entrance Surface Air Kerma (ESAK) was measured with an RTI PIRANHA X-ray multimeter. The images were evaluated as presented to the dentist by the detector software, in 12bit format. The resolution of the detector was found better than 100 μm. The DQE curves suggested optimum exposure conditions below 133 μGy.

1. Introduction

Digital radiology is the state of the art method for mapping the spatial distribution of different elemental components in human tissues [1–5]. A subspecialty of digital imaging is dental imaging. It is performed by dedicated X-ray instrumentation either in panoramic or intraoral mode [6–14]. The radiation burden to the patient imposes optimization of the radiographic procedure, without degrading image quality standards [15–21]. In recent years digital radiography is the standard dental imaging method [13,14,18,22,23], compared to the previously used X-ray films [22]. The backbone of dental imaging is the type of X-ray detector, whose characteristics affect the quality of the final image. Published literature assessment of the performance of intraoral X-ray detectors [23,24] has been achieved using objective measures such as X-ray sensitivity, contrast and resolution [9,11,13,25–29]. In addition, studies regarding the subjective image perception of dental radiographs have been published [20,30,31]. A point worth discussing in the aforementioned studies is the detector characterization in the spatial frequency domain. To this end the Modulation Transfer Function (MTF) [2–4,32–34] showing in effect the capability of a system to retain high contrast information to small image sizes has been investigated [10,26–28,35,36]. To fully evaluate X-ray imaging detectors, additionally objective measurements have been proposed. Such measurements are the Normalize Noise Power Spectra (NNPS) showing the relative noise variation in the spatial frequency domain and the Detective Quantum Efficiency (DQE), which is a measure of the signal-to-noise squared transfer from the input to the output of the detector. DQE as expressed in the spatial frequency domain is a function of the MTF, the NNPS and the incident number of X-ray photons. Thus it can be considered as an objective parameter for determining the overall performance of an X-ray detector. The use of DQE for assessing the performance of digital detectors for radiographic applications is used extensively [14,37–44]. An evaluation in the spatial frequency domain, through MTF and NNPS, has been reported for a SCHICK CDR2000 DICOM detector at 8 bit digitization mode [45,46]. In addition the MTF and DQE at 8 bit at 60 kVp X-ray tube voltage have been investigated [14]. However as far as our knowledge of current literature allows, we have not found any work studying the overall performance of a SCHICK

* Corresponding author.
E-mail address: nkalyvas@uniwa.gr (N. Kalyvas).

https://doi.org/10.1016/j.measurement.2019.107171
0263-2241/

CDR2000 digital dental detectors in terms of MTF, noise and DQE in 12bit mode, both at 60kVp and 70 kVp irradiation conditions. In this work the performance evaluation in spatial frequency domain of an intraoral digital detector (SCHICK CDR2000 DICOM) in terms of MTF, DQE and noise, in 12 bit mode, for two different X-ray tube voltages of dental interest is presented. An Active Pixel Sensor (APS) Complementary Metal Oxide Semiconductor (CMOS) X-ray sensor with 40 μm pixel [46] size as the one studied here may be of interest in applications beside dental imaging, like small animal imaging were X-ray tube voltages between 60kVp and 70 kVp are of interest.

2. Material and methods

A digital dental detector SCHICK CDR DICOM with serial number 540820 was investigated [46]. The detector consists of a scintillator (indirect detection) in contact with a CMOS array. The pixel size was 40 μm. No information was available in the manufacturer specification regarding the scintillation type and thickness. However to our knowledge the scintillator usually used in digital X-ray imaging are either CsI:Tl columnar phosphors or Gd_2O_2S based phosphors in granular form [1]. The year this type of detector was designed (that is 2005) makes more prominent the use of the Gd_2O_2S scintillator. The irradiation conditions comprised a radiographic X-ray unit BMI General Medical Merate with a rotated anode of 0.6 mm focal spot size and inherent Al filtration of 2 mm. The small focal spot of the X-ray tube was utilized. The focus to detector distance was 150 cm. The exposure protocol comprised measurements at 60kVp and 70 kVp to simulate the peak voltages currently used in intraoral dental imaging [9]. The mAs used in this study are in the range 5.6 mAs to 12.5 mAs. The digital image was captured and digitized by the detector available software. Images of 12 bit, with a sinusoidal map and an inverted Look-Up Table (LUT) both applied by the detector software, were obtained and evaluated. All the frequency related parameters (MTF, NNPS and DQE) were calculated by means of a validated free available plugin, according to International Electrotechnical Commission (IEC) methodology, named COQ [37], which can be found online (www.medphys.it/downloads.htm), created for ImageJ software [47].

2.1. Sensitivity

The sensitivity of the detector is expressed in terms of the Mean Pixel Value (MPV) as a function of the incident Entrance Surface Air Kerma (ESAK). The ESAK incident on the detector, measured with a Piranha (RTI) multimeter, was in the range from 66 μGy to 210 μGy, similar to ESAK values reported in literature [36,44,48]. The MPV for the different ESAK values was calculated by means of ImageJ software [47].

2.2. MTF

The Modulation Transfer Function describes the capability of the detector to resolve details of adjacent high contrast objects. It corresponds to the signal transfer function of the system. It is customary to define the resolution of the detector at spatial frequencies corresponding to the 10% or lower of the maximum of the MTF. The MTF of the digital detector was found in terms of the Edge Response Function or Edge Spread Function (ESF) [37,38,41]. A tungsten edge test device, supplied by the PTW Freiburg Company, was used to obtain slanted images in both 60 kVp and 70 kVp tube voltages at an ESAK value corresponding to the linear part of the response curve previously obtained. The edge test device consists of a 1 mm thick W edge plate (100×75 mm^2) fixed on a 3 mm thick lead plate. The ESF was calculated, by irradiating the 1 mm nominal thickness W part of the edge, at a symmetrical Region of Interest (ROI) around the edge image. Then the ESF was differentiated to obtain the line spread function (LSF). Finally, the normalized LSF was Fourier transformed to give the pre-sampling MTF [37].

2.3. Noise

2.3.1. NNPS

The Normalized Noise Power Spectrum (NNPS) was calculated on the uniform exposed images, corresponding to the linear part of the detector response curve, with ESAK values around 100 μGy. The image was subdivided into 128 × 128 half overlapping ROIs. In each ROI the pixel value deviation from the mean was obtained. This yielded a map of the signal differences. This map was Fourier Transformed and squared, in order to obtain the spectral components of the signal spatial variations, corresponding to the noise power spectrum (NPS). NNPS was obtained by dividing NPS by the square of the corresponding mean signal value (MSV), $NNPS(f) = NPS(f)/(MSV)^2$, where f is the spatial frequency, and afterward the ensemble average, by considering all ROIs, was obtained [37,38].

2.3.2. NTF

The knowledge of NNPS enables the calculation of the Noise Transfer Function, NTF, showing the image noise transfer characteristics of the detector, defined as [49]:

$$NTF^2(f) = \frac{NPS(f)}{NPS(0)} \tag{1a}$$

By taking into consideration that *NNPS(f)* is the Noise Power spectrum divided by the square of the mean signal value, it can be derived that:

$$NTF(f) = \sqrt{\frac{NNPS(f)}{NNPS(0)}} \tag{1b}$$

2.4. DQE

The DQE of the system describes the ratio of the output over the input signal-to-noise squared. In the spatial frequency domain it can be expressed in terms of MTF, NNPS and ESAK as follows [37–40]:

$$DQE(f) = \frac{[MTF(f)]^2}{ESAK \cdot q \cdot NNPS(f)} \tag{2}$$

where q is the number of X-ray *photons*/(mm^2μGy). The product *ESAK* q (photons/mm^2) corresponds to the square of the input Signal-to-Noise ratio. For the calculation of Eq. (2) parameter q was obtained by an online X-ray spectra simulation tool [50]. This tool is based in published literature [51,52] and generates radiographic spectra (photons/mm^2μ*Gy*) in energy bins of 1 keV. In order to obtain the number of photons/mm^2μ*Gy* required for the calculation of DQE, (i) we summed the photons of the X-ray spectra, (ii) calculate per energy bin the radiation exposure by means of a method described in literature [53] and summed over all the spectrum energy bins. The air mass energy absorption coefficient required was found by XmuDat software [54]. The value of q was determined by dividing the number of photons of the spectrum with the radiation exposure expressed in μGy. Specifically for 60kVp, q was calculated as 16,300 photons/mm^2μGy and for 70 kVp, q was calculated as 18,300 photons/mm^2μGy [53,55].

3. Results and discussion

In Fig. 1, the dental detector response curves, for 60 kVp and 70 kVp exposure conditions, are demonstrated. 60 kVp data is shown in rhombus, while the 70 kVp data are shown in squares. It may be seen that the detector exhibits linear exposure response for the ESAK values under consideration. The fitted equation for 60 kVp is $MPV = 16.158 \cdot ESAK - 661.9$ and for 70 kVp is $MPV = 18.105 \cdot ESAK - 837.29$. The slope of the two curves is very similar. In Fig. 2 the corresponding MTF curves are demonstrated for 60 kVp and 70 kVp. By inspecting the MTF curves it can be shown that the 10% of maximum MTF corresponds to 10 mm^{-1}. This value, which corresponds to sizes of 100 μm, may be adopted in practice as an estimation of the detector's spatial resolution. The resolution limit of the detector under investigation is its pixel size (40 μm). By applying the Nyquist theorem it is deduced that sizes of the order of 80 μm can be accurately resolved. This value corresponds to a spatial frequency of 12.5 mm^{-1}, a value very close to the 5% of the calculated MTF curves. A point worth commenting is that the MTF values at 60kVp and 70 kVp are very similar. This may be attributed to the small difference of the ESAK values as well as the relative similarity of the X-ray spectra. More specifically the average energy of the 60 kVp spectrum was estimated 37.132 keV, while the average energy of the 70 kVp spectrum was estimated 40.782 keV [51,55]. Such small keV differences are not expected to yield substantial changes in the X-ray interaction depth within the scintillator, thus no substantial difference in the scintillator's light output [56] or in the MTF is expected.

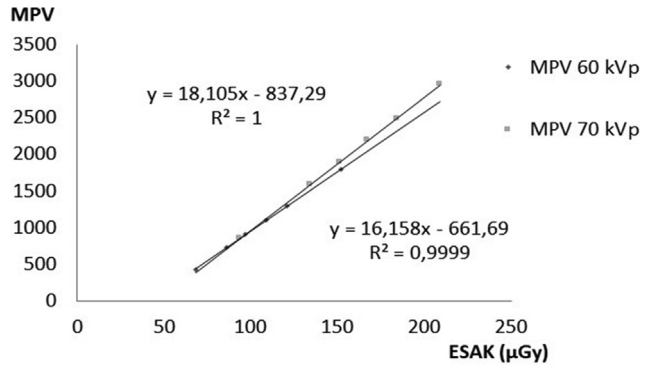

Fig. 1. The detector response curve (12 bit image) for different ESAK values, at 60kVp and 70 kVp.

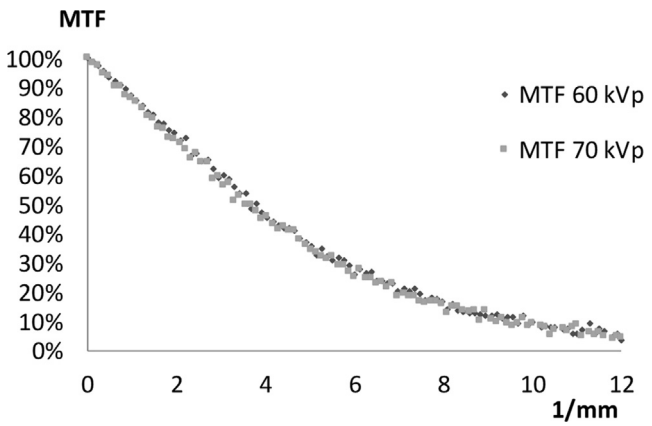

Fig. 2. The detector MTF at 60kVp for 109 μGy and at 70 kVp for 93 μGy.

In Fig. 3a the corresponding NNPS curves are demonstrated. The presented curves have many similarities, implying that for the sensor settings applied the relative noise fluctuations are comparable. In addition in Fig. 3b the related NTF curves are also shown. The shape of the NTF curve is generally affected by the shape of the corresponding MTF curve, since random noise is transferred through the system's transfer function. Noise however is transferred more effectively than the signal at higher spatial frequencies. This is evident from Fig. 3b, where NTF values at the resolution limits of the detector are above 0.2. This value may incorporate electronic or thermal noise sources which are not zero [29,30,35]. It is interesting to notice that the 60kVp image presents lower noise value than the 70 kVp image. Noise for the same detector is affected by the relative X-ray absorption capability of the detector as well as the incident exposure. Higher exposure provides more signal carriers thus lower noise. In our case the difference in NNPS for 60 kVp and 70 kVp exposure conditions is a combination of the X-ray absorption capability of the detector and the number of the X-rays incident on the detector surface. The latter can be obtained by the multiplication of *ESAK* with *q*. The product $ESAK \cdot q$ for 60 kVp is approximately *1,776,700 photons/mm²* and for 70kVp is approximately *1,701,900 photons/mm²*. In Fig. 4 the simulated X-ray spectra of 60 kVp and 70 kVp [36], as well as the X-ray mass attenuation coefficients of CsI and Gd_2O_2S scintillators, obtained by XmuDat software package [41], are demonstrated. It can be seen that both X-ray spectra equivalently meet the absorption coefficients of the scintillator materials used in the indirect CMOS detector.

In Fig. 5 the detector DQE is demonstrated for both 60 kVp and 70 kVp. DQE values were calculated in terms of equation (2), thus the shape of the DQE curves are a function of the MTF and NNPS. In Figs. 6a and 6b the DQE of the detector at 60 kVp and 70 kVp

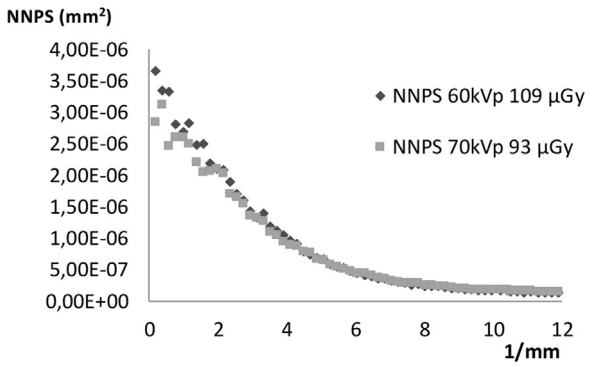

Fig. 3a. The detector NNPS at 60kVp for 109 μGy and at 70 kVp for 93 μGy.

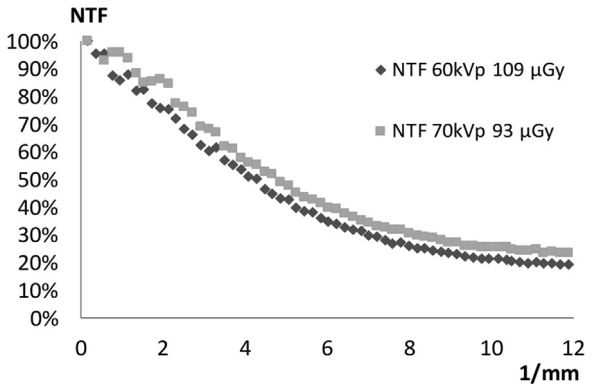

Fig. 3b. The detector NTF at 60kVp for 109 μGy and at 70 kVp for 93 μGy.

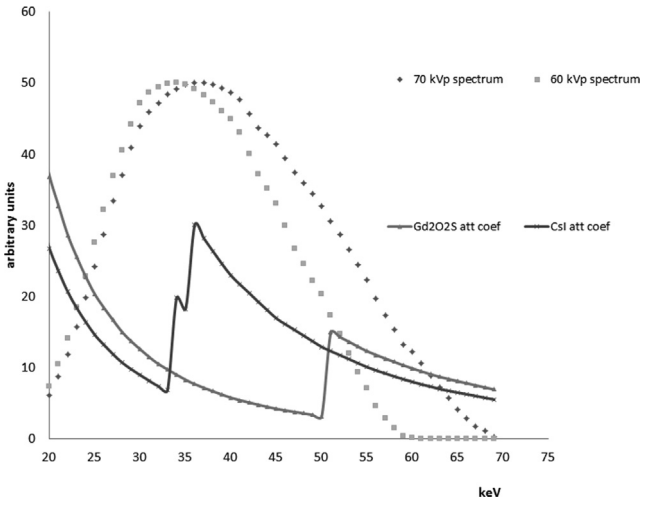

Fig. 4. The X-ray spectra used and the mass attenuation coefficients of the scintillators that can be utilized with the SCHICK CDR detector.

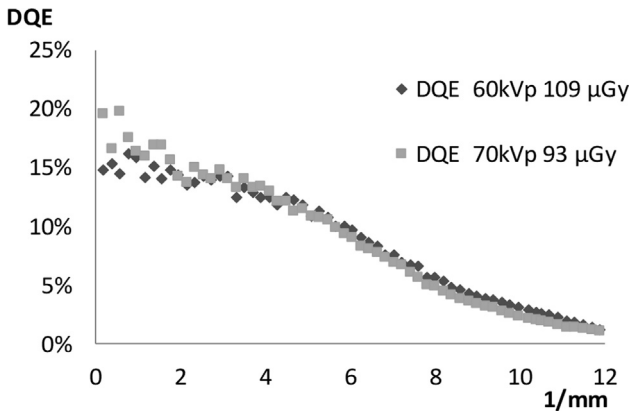

Fig. 5. The detector DQE at 60kVp for 109 μGy and at 70 kVp for 93 μGy.

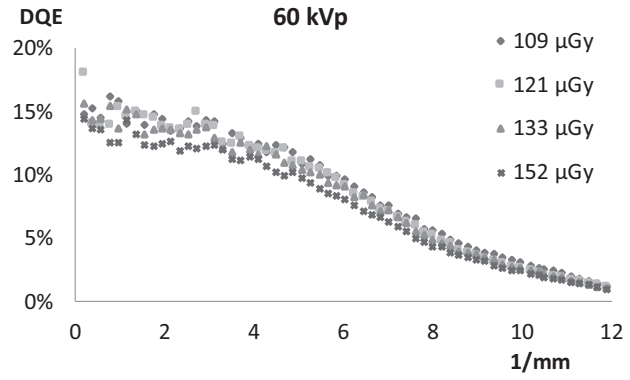

Fig. 6a. The detector DQEs at 60kVp and for different ESAK values.

respectively for different ESAK values are shown. The inspection of Fig. 6a shows no DQE differences from 109 to 133 μGy and lower DQE values for ESAK values of 152 μGy. Furthermore, Fig. 6b suggests that an optimum DQE is calculated for the 93 μGy ESAK value. Differences in DQE with ESAK for intraoral dental detectors have been also reported in literature [14,44]. Our DQE results suggest that the detector can perform optimal for ESAK values up-to 133 μGy. Higher exposure at the detector surface will not improve either image quality or the information available to the dentist.

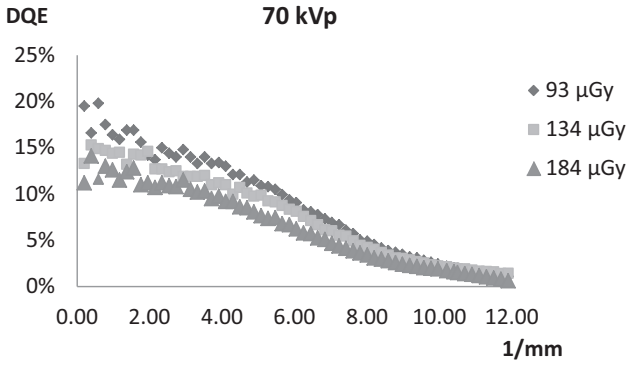

Fig. 6b. The detector DQEs at 70kVp and for different ESAK values.

This is of great importance in radiation protection of the patients as well as the dentists. Published literature regarding Diagnostic Reference Levels (DRL) at the output of the collimator end reports ESAK values from 0.95 mGy up to 4.0 mGy [15]. The ESAK incident on the detector surface depends upon tissue thickness and the tooth type [12,15]. If the SCHICK APS detector presented in this study is utilized, then the X-ray exposure conditions should be optimized so the ESAK on the detector surface should not exceed 133 μGy.

By comparing the MTF results of this work with the MTF results of a similar SCHICK detector with serial number 540957 [32], presented in 8 bit image format, it is shown that the MTF curve is similar to the one presented here. The corresponding pixel value response curves were presented saturated near the 255 pixel value. Finally the NNPS values of the 540,957 detector (8 bit image) were measured higher than the ones presented in this work (12 bit image). The higher NNPS of the 8 bit image is more likely to be attributed to differences of the 8 bit image quantization process compared to the corresponding 12 bit image format. In addition, our results compared to a SCHICK CDR2000 dental detector irradiated at 60 kVp, 8bit conditions [14] present similar MTF curves. The response curve in our case demonstrates linear behavior for higher ESAK values. The DQE curve at 60 kVp 109 μ*Gy*, 12 bits, presented in this study is similar in shape with the corresponding DQE curve, 8 bit 104 μ*Gy* presented by Tsusida et al [14], up to 6 lp/mm spatial frequency. For higher frequencies however our corresponding DQE values are lower. This may be attributed to the difference in quantization bits and the mapping applied by the software in this study. Our MTF results are better or comparable, from the ones presented in literature for a Charge-Coupled Device (CCD) intraoral sensor coupled with various scintillators [36]. When the corresponding DQE curves are considered [44], our results present higher DQE values compared to the CCD/Gd_2O_2S intraoral detector combination and similar with the CCD/CsI intraoral detector combination. The DQE results presented in this work however are inferior to the corresponding CCD/LuAG:Ce combination results [44]. Our DQE values, for 70 kVp and ESAK 93 μGy, were compared with published results for a RadEye CMOS digital sensor, having a pixel size of 22.5 μm coupled with two scintillator detectors: (i) a 33.91 mg/cm^2 Gd2O2S:Tb, commercially available scintillator screen [24] and (ii) a 65.1 mg/cm^2 Gd2O2S:Eu screen [25]. Our results were found poorer than both combinations. The last combination however (i.e. the 65.1 mg/cm^2 Gd_2O_2S:Eu screen) for higher ESAK values performs poorer than the SCHICK detector. The comparison of the presented DQE results with the DQE obtained by two CsI:Tl detectors coupled to the RadEye CMOS [26], shows that the SCHICK detector performs better than 140 μm and 170 μm CsI:Tl/CMOS detector combinations for low frequency values. However, for higher spatial frequencies the aforementioned CsI:

Tl/RadEye detectors prevail. Their improved performance may be attributed to the possible scintillator type and thickness differences, to the X-ray spectrum differences, as well as, to the smaller pixel size of RadEye, which enables it to resolve higher spatial frequencies. Besides the differences between the kVp values, the bit value and the exposure conditions, the presented results in the spatial frequency domain may be affected by a penumbra component superimposed by the thickness of the edge device.

4. Conclusion

The image quality and transfer characteristics of SCHICK CDR digital dental detector were studied by parameters like the pixel value response, the Modulation Transfer Function, the Normalized Noise Power Spectrum, the Noise Transfer Function and the Detective Quantum Efficiency, at 60 kVp and 70 kVp covering the range of intraoral X-ray equipment. For both X-ray tube voltages it was found that the detector could resolve sizes up to 80 μm (corresponding to approximately 5% of the MTF curve). The optimum ESAK values of the detector were found below 133 μGy. The DQE is slightly higher at 70 kVp for spatial frequencies smaller than 5 mm^{-1}. For higher spatial frequencies the detector presents better DQE at 60 kVp irradiation conditions.

Declaration of Competing Interest

The authors declare that they have no known competing financial interests or personal relationships that could have appeared to influence the work reported in this paper.

References

[1] Horst Aichinger, Joackim Dierker, Sigrid Joite-Barfuβ, Manfred Sabel, Radiation Exposure and Image Quality in X-ray Diagnostic Radiology, Physical Principles and Clinical Applications, Second Edition, Springer ISBN 978-3-642-11240-9, DOI10.1007/978-3-642-11241-6 Springer Heidelberg Dordrecht London New York copyright Springer-Verlag Berlin Heidelberg, 2012.

[2] G. Andria, F. Attivissimo, G. Guglielmi, A.M.L. Lanzolla, A. Maiorana, M. Mangiantini, Towards patient dose optimization in digital radiography, Measurement 79 (2016) 331–338.

[3] S.E. Bohndiek, A. Blue, J. Cabello, A.T. Clark, N. Guerrini, P.M. Evans, E.J. Harris, A. Konstantinidis, D. Maneuski, J. Osmond, V. O'Shea, R.D. Speller, R. Turchetta, K. Wells, H. Zin, N.M. Allinson, Characterization and testing of LAS: A prototype 'large area sensor' with performance characteristics suitable for medical imaging applications, IEEE Trans. Nucl. Sci. 56 (5) (2009) 2938–2946.

[4] C. Zhao, J. Kanicki, A.C. Konstantinidis, T. Patel, Large area CMOS active pixel sensor x-ray imager for digital breast tomosynthesis: analysis, modeling, and characterization, Med. Phys. 42 (2015) 6294–6308.

[5] Shibiao Tang, Jiabao Xie, Qingli Ma, Plastic scintillation fiber array coupling CCD for X-ray imaging and detection, Measurement 42 (2009) 933–936.

[6] Djordje Antonijević, Dragan Ilić, Vesna Medić, Slobodan Dodić, Kosovka Obradović-Djuričić, Zoran Rakočević, Evaluation of conventional and digital radiography capacities for distinguishing dental materials on radiograms depending on the present radiopacifying agent, Vojnosanit Pregl 71 (11) (2014) 1006–1012.

[7] V. Tsapaki, Radiation protection in dental radiology – Recent advances and future directions, Physica Med. 44 (2017) 222–226.

[8] U. Welander, P. Nelvig, G. Tronje, W.D. McDavid, B. Dove, A.C. Mörner, T. Cederlund, Basic technical properties of a system for direct acquisition of digital intraoral radiographs, Oral Surg Oral Med, Oral Pat. 75 (1993) 506–516.

[9] D. Mondou, E. Bonnet, J.L. Coudert, M. Jourlin, R. Molteni, V. Pachod, Criteria for the assessment of intrinsic performances of x-ray digital intra-oral sensors, applied to Gendex Visualix, Acad Radiol 3 (1996) 51–757.

[10] S.K. Chen, L. Hollender, Modulation transfer function of a digital dental x-ray system, Oral Surg. Oral Med. Oral Pathol. Oral Radiol. Endod. 77 (1994) 308–313.

[11] K. Araki, A. Endo, T. Okano, An objective comparison of four digital intra-oral radiographic systems: sensitometric properties and resolution, Dentomaxillofacial Radiology 29 (2000) 76–80.

[12] A.G. Farman, T.T. Farman, A comparison of 18 different x-ray detectors currently used in dentistry, Oral Surg. Oral Med. Oral Pathol. Oral Radiol. Endod. 99 (2005) 485–489.

[13] S. Teich, W. Al-Rawi, M. Heima, F.F. Faddoul, G. Goldzweig, Z. Gutmacher, D. Aizenbud, Image quality evaluation of eight CMOS (Complementary Metal-Oxide Semiconductor) intraoral digital x-ray sensors, Int Dent J. 66 (2016) 264–271.

[14] R. Tsuchida, A. Kazuyuki, A. Endo, I. Funahashi, T. Okano, Physical properties and ease of operation of a wireless intraoral x-ray sensor, Oral Surg Oral Med Oral Pathol Oral Radiol Endod. 100 (2005) 603–608.

[15] G. Manousaridis, C. Koukorava, C.J. Hourdakis, V. Kamenopoulou, E. Yakoumakis, K. Tsiklakis, Establishment of diagnostic reference levels for dental intraoral radiography, Radiat. Prot. Dosim. 156 (2013) 455–457.

[16] G. Manousaridis, C. Koukorava, C.J. Hourdakis, V. Kamenopoulou, E. Yakoumakis, K. Tsiklakis, Establishment of diagnostic reference levels for dental panoramic radiography in Greece, Radiat. Prot. Dosim. 165 (2015) 111–114.

[17] AAPM report No 175, Acceptance Testing and Quality Control of Dental Imaging Equipment", The Report of AAPM Task Group 175 September 2016, 2016 by American Association of Physicists in Medicine. ISSN: 0271-7344, Published by American Association of Physicists in Medicine 1631 Prince Street Alexandria, VA 22314-2818.

[18] P. Mah, W. Doss McDavid, S. Brent Dove, Quality assurance phantom for digital dental imaging, Oral Surg. Oral Med. Oral Pathol. Oral Radiol. Endod. 112 (2011) 632–639.

[19] European Commission, RADIATION PROTECTION N° 162, "Criteria for Acceptability of Medical Radiological Equipment used in Diagnostic Radiology, Nuclear Medicine and Radiotherapy" Directorate-General for Energy Directorate D — Nuclear Safety & Fuel Cycle Unit D4 — Radiation Protection, 2012.

[20] M.H. Nassef, Image Quality Assessment and Radiation exposure in Intra Oral Dental Radiography, Int. J. Innovat. Educat. Res. 5 (2) (2017).

[21] IAEA HUMAN HEALTH SERIES No. 28 Worldwide Implementation of Digital Imaging in Radiology, a Resource Guide in Cooperation with the World Health Organization, © IAEA, 2015 Printed by the IAEA in Austria January, 2015 STI/PUB/1647.

[22] J. A. Wallace, M. K. Nair, M. F. Colaco and S. F. Kapa, A comparative evaluation of the diagnostic efficacy of film and digital sensors for detection of simulated periapical lesions Oral Surg. Oral Med. Oral Pathol., doi: 10.1067/moe.2001.115974.

[23] G.J. Christensen, Digital radiography sensors: which is the best?, Clinicial Report 4 (9) (2011) 1–3.

[24] W. Al-Rawi, S. Teich, Evaluation of physical properties of different digital intraoral sensors, Compendium of continuing education in dentistry, 34 (8), 2013, e76–e83.

[25] H. Udupa, P. Mah, S.B. Dove, W.D. McDavid, Evaluation of image quality parameters of representative intraoral digital radiographic systems, Oral Surg. Oral Med. Oral Pathol. Oral Radiol. 116 (6) (2013) 774–783.

[26] D.D. Brüllmann, B. Kempkes, B. d'Hoedt, R. Schulze, Contrast curves of five different intraoral X-ray sensors: a technical note, Oral Surg. Oral Med. Oral Pathol. Oral Radiol. 115 (6) (2013) e55–e61.

[27] K. Hellén-Halme, C. Johansson, M. Nilsson, Comparison of the performance of intraoral X-ray sensors using objective image quality assessment, Oral Surg. Oral Med. Oral Pathol. Oral Radiol. 121 (5) (2016) e129–e137.

[28] A.G. Attaelmanan, E. Borg, H.-G. Gröndahl, Assessments of the physical performance of 2 generations of 2 direct digital intraoral sensors, Oral. Surg. Oral. Med. Oral. Pathol. Oral. Radiol. Endod. 88 (1999) 517–523.

[29] D.D. Brüllmann, B. Kempkes, R. Schulze, Contrast curves of five different intraoral X-ray sensors: a technical note, Oral Surg. Oral Med. Oral Pathol. Oral Radiol. 115 (2013) e55–e61.

[30] A.G. Attaelmanan, E. Borg, H.-G. Gröndahl, Signal-to-noise ratios of 6 intraoral digital sensors, Oral. Surg. Oral Med. Oral. Pathol. Oral. Radiol. Endod. 91 (2001) 611–615.

[31] G.C.H. Sanderink, P.F. van der Stelt, U.S. Welander, S.E. Stheeman, Image quality of direct digital intraoral x-ray sensors in assessing root canal length, Oral Surgery Oral Medicine Oral, Pathology 78 (1994) 125–132.

[32] P.B. Greer, T. van Doorn, Evaluation of an algorithm for the assessment of the MTF using an edge method, Med. Phys. 27 (2000) 2048–2059.

[33] J.R. Wells, J.T. Dobbins, Estimation of the two-dimensional presampled modulation transfer function of digital radiography devices using one-dimensional test objects, Med. Phys. 39 (2012) 6148–6160.

[34] D.D. Brüllmann, B. d'Hoedt, The modulation transfer function and signal-to-noise ratio of different digital filters: a technical approach, Dentomaxillofac. Radiol. 40 (2011) 222–229.

[35] U. Welander, W.D. McDavid, G.C.H. Sanderink, G. Tronje, A.C. Mörner, B. Dove, Resolution as defined by line spread and modulation transfer functions for four digital intraoral radiographic systems, Oral Surg. Oral Med. Oral Pathol. Oral Radiol. Endod. 78 (1994) 109–115.

[36] T.T. Farman, R.H. Vandre, J.C. Pajak, S.R. Miller, A. Lempicki, A.G. Farman, Effects of scintillator on the modulation transfer function (MTF) of a digital imaging system, Oral Surg. Oral Med. Oral Pathol. Oral Radiol. Endod. 99 (2005) 608–613.

[37] B. Donini, S. Rivetti, N. Lanconelli, M. Bertolini, Free software for performing physical analysis of systems for digital radiography and mammography, Med. Phys. 41 (5) (2014), 051903-1 up to 51903-10.

[38] C.M. Michail, V.A. Spyropoulou, G.P. Fountos, N.I. Kalyvas, I.G. Valais, I.S. Kandarakis, G.S. Panayiotakis, Experimental and theoretical evaluation of a high resolution CMOS based detector under X-ray imaging conditions, IEEE Trans. Nucl. Sci. 58 (1) (2011) 314–322.

[39] I.E. Seferis, C.M. Michail, I.G. Valais, G.P. Fountos, N.I. Kalyvas, F. Stromatia, G. Oikonomou, I.S. Kandarakis, G.S. Panayiotakis, On the response of europium doped phosphor-coated CMOS digital imaging detector, Nucl. Instrum. Method. Phys. Res. A 729 (2013) 307–315.

[40] C. Michail, I. Valais, I. Seferis, N. Kalyvas, G. Fountos, I. Kandarakis, Experimental measurement of a high resolution CMOS detector coupled to CsI scintillators under X-ray radiation, Radiat. Meas. 74 (2015) 39–46.
[41] C. Michail, I. Valais, N. Martini, V. Koukou, N. Kalyvas, A. Bakas, I. Kandarakis, G. Fountos, Determination of the detective quantum efficiency (DQE) of CMOS/CsI imaging detectors following the novel IEC 62220-1-1:2015, Int. Stand. Radiat. Meas 94 (2016) 8–17.
[42] M. Esposito, T. Anaxagoras, A.C. Konstantinidis, Y. Zheng, R.D. Speller, P.M. Evans, N.M. Allinson, K. Wells, Performance of a novel wafer scale CMOS active pixel sensor for bio-medical imaging, Phys. Med. Biol. 59 (13) (2014) 3533–3554.
[43] U. Welander, W.D. McDavid, A.-K. Mörner, Gunilla Tronje, Osamu Tokuoka, Hajime Fuchihata, Per Nelvig, S. Brent Dove, Absolute measures of image quality for the Sens-A-Ray direct digital intraolral radiography system, Oral. Surg. Oral. Med. Oral. Pathol. Oral. Radiol. Endod. 80 (1995) 345–350.
[44] T.T. Farman, R.H. Vandre, J.C. Pajak, S.R. Miller, A. Lempicki, A.G. Farman, Effects of scintillator on the detective quantum efficiency (DQE) of a digital imaging system, Oral Surg. Oral Med. Oral Pathol. Oral Radiol. Endod. 101 (2006) 219–223.
[45] A. Anastasiou, C. Michail, V. Koukou, N. Martini, A. Bakas, F. Papastamati, P. Maragkaki, L. Lavdas, G. Fountos, I. Valais, N. Kalyvas, Examining the Spatial Frequency Components of a Digital Dental Detector, IOP Conf. Series: J. Phys. Conf. Series 931 (2017), 012005.
[46] Schick Technologies, Inc. 2009: "Schick/CDR DICOM/English Edition", https://www.schickbysirona.com/items.php?catid=408. (last accessed February 2019)
[47] ImageJ 1.47h, Wayne Rasband, National Institute of Heallth, USA https://imagej.nih.gov/ij/
[48] S.-K. Chen, L. Hollender, Detector response and exposure control of the Radio VisioGraphy system (RVG 32000 ZHR) Oral and Maxillofacial, Radiology 76 (1993) 104–111.
[49] N. Kalivas, L. Costaridou, I. Kandarakis, D. Cavouras, C.D. Nomicos, G. Panayiotakis, Modeling quantum and structure noise of phosphors used in medical x-ray imaging detectors, Nucl. Instrum. Method. Phys. Res. A 490 (2002) 614–629.
[50] https://www.oem-xray-components.siemens.com/x-ray-spectra-simulation (last accessed March 2019).
[51] John M. Boone, Thomas R. Fewell, Robert J. Jennings, Molybdenum, rhodium, and tungsten anode spectral models using interpolating polynomials with application to mammography, Med. Phys. 24 (12) (1997) 1883–11874.
[52] M. John, J. Boone, Anthony Seibert: an accurate method for computer-generating tungsten anode x-ray spectra from 30 to 140 kV, Med. Phys. 24 (11) (1997) 1661–1670.
[53] L. Abbene, A. La Manna, F. Fauci, G. Gerardi, S. Stumbo, G. Raso, X-ray spectroscopy and dosimetry with a portable CdTe device, Nucl. Instrum. Meth. Phys. Res. A 571 (2007) 373–377.
[54] Nowotny R. 1998. "XMuDat: Photon attenuation data on PC", International Atomic Energy Agency, Nuclear Data Section, https://www-nds.iaea.org/publications/iaea-nds/iaea-nds-0195.htm, (last accessed February 2019).
[55] A.R. El-Sersy, N.R. Khalel, N.E. Khaled, S.A. Eman, H.M. Eissa, Characterization study on NIS X-ray beam qualities and its applications, Measurement 45 (2012) 1301–1307.
[56] C. Michail, I. Valais, G. Fountos, A. Bakas, C. Fountzoula, N. Kalyvas, A. Karabotsos, I. Sianoudis, I. Kandarakis, Luminescence efficiency of calcium tungstate (CaWO4) under X-ray radiation: Comparison with Gd2O2S:Tb, Measurement 120 (2018) 213–220.